

Endogenous Labile Iron Pool-Mediated Free Radical Generation for Cancer Chemodynamic Therapy

Lisen Lin,[†] Sheng Wang,[†] Hongzhang Deng, Weijing Yang, Lang Rao, Rui Tian, Yuan Liu, Guocan Yu, Zijian Zhou, Jibin Song, Huang-Hao Yang, Zhi-Yi Chen,* and Xiaoyuan Chen*

Cite This: *J. Am. Chem. Soc.* 2020, 142, 15320–15330

Read Online

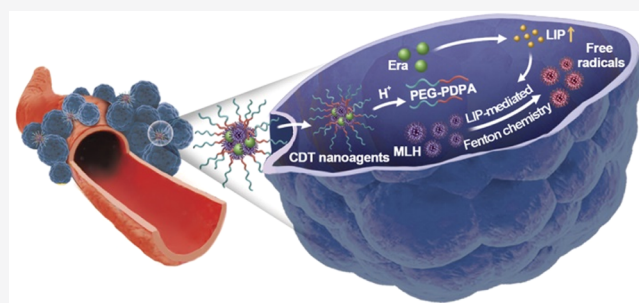
ACCESS |

Metrics & More

Article Recommendations

Supporting Information

ABSTRACT: Current chemodynamic therapy (CDT) primarily relies on the delivery of transition metal ions with Fenton activity to trigger hydroxyl radical production from hydrogen peroxide. However, administration of an excess amount of exogenous Fenton-type heavy metals may cause potential adverse effects to human health, including acute and chronic damages. Here, we present a new CDT strategy that uses intracellular labile iron pool (LIP) as the endogenous source of Fenton-reactive metals for eliciting free radical generation, and the discovery of hydroperoxides (R'OOH) as an optimal LIP-mediated chemodynamic agent against cancer. By simulating the metabolic fates of peroxy compounds within cells, R'OOH was found to have excellent free radical-producing ability in the presence of labile iron(II) and to suffer only moderate elimination by glutathione/glutathione peroxidase, which contributes to its superior chemodynamic efficacy. The LIP-initiated nontoxic-to-toxic transition of R'OOH, together with increased LIP levels in tumor cells, enabled efficient and specific CDT of cancer. Moreover, pH/labile iron(II) cascade-responsive nanomedicines comprising encapsulated methyl oleolate hydroperoxide and LIP-increasing agent in pH-sensitive polymer particles were fabricated to realize enhanced CDT. This work not only paves the way to using endogenous Fenton-type metals for cancer therapy but also offers a paradigm for the exploration of high-performance chemodynamic agents activated by intracellular LIP.



INTRODUCTION

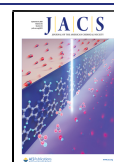
Chemodynamic therapy (CDT), which employs Fenton chemistry involving the reaction of Fenton-active metals with peroxide groups to produce highly deleterious reactive oxygen species (ROS), is regarded as a promising strategy for cancer treatment.^{1–9} The ROS generation by Fenton-type reactions depends on neither molecular oxygen (O₂) nor external light source, enabling CDT to avoid the major shortcomings of photodynamic therapy in which ROS formation is strongly inhibited by tumor hypoxia and limited light penetration depth.^{10–18} Despite its great therapeutic potential, CDT technology remains in its infancy. Currently, the main approach used in CDT of tumor is to deliver low-valent transition metal ions with high Fenton activity for triggering the conversion of intracellular hydrogen peroxide (H₂O₂) into highly reactive hydroxyl radicals that have been proposed to induce oxidative stress and subsequent cancer cell death through the oxidation of various biomolecules such as lipids, proteins, and DNA.^{19–28} Nevertheless, one major concern of this method is that exogenous administration of excess Fenton-type heavy metals such as iron, manganese, copper, and cobalt may cause potential adverse effects to human health, including acute and chronic toxicity. Therefore, the development of an

alternative strategy to circumvent this issue in CDT is highly desirable.

As the most abundant transition metal in biological systems, iron plays an essential role in numerous cellular metabolic processes, such as DNA synthesis, cell cycle regulation, and cell proliferation.²⁹ Especially, a small part of free or loosely bound intracellular iron(II), referred to as the labile iron pool (LIP),³⁰ is redox-active and thus possesses the capability of participating in the Fenton-type reactions within cells to generate free radicals. More importantly, cancer cells not only have a higher need for iron than their normal counterparts in order to sustain their rapid proliferation but also exhibit upregulated expression of transferrin receptor 1 and hepcidin along with down-regulated expression of ferroportin, giving rise to substantially increased level of LIP in cancerous tissues.^{31–34} From this perspective, intracellular LIP of tumor cells appears to be a potential endogenous source of Fenton-reactive iron(II) for

Received: May 22, 2020

Published: August 21, 2020



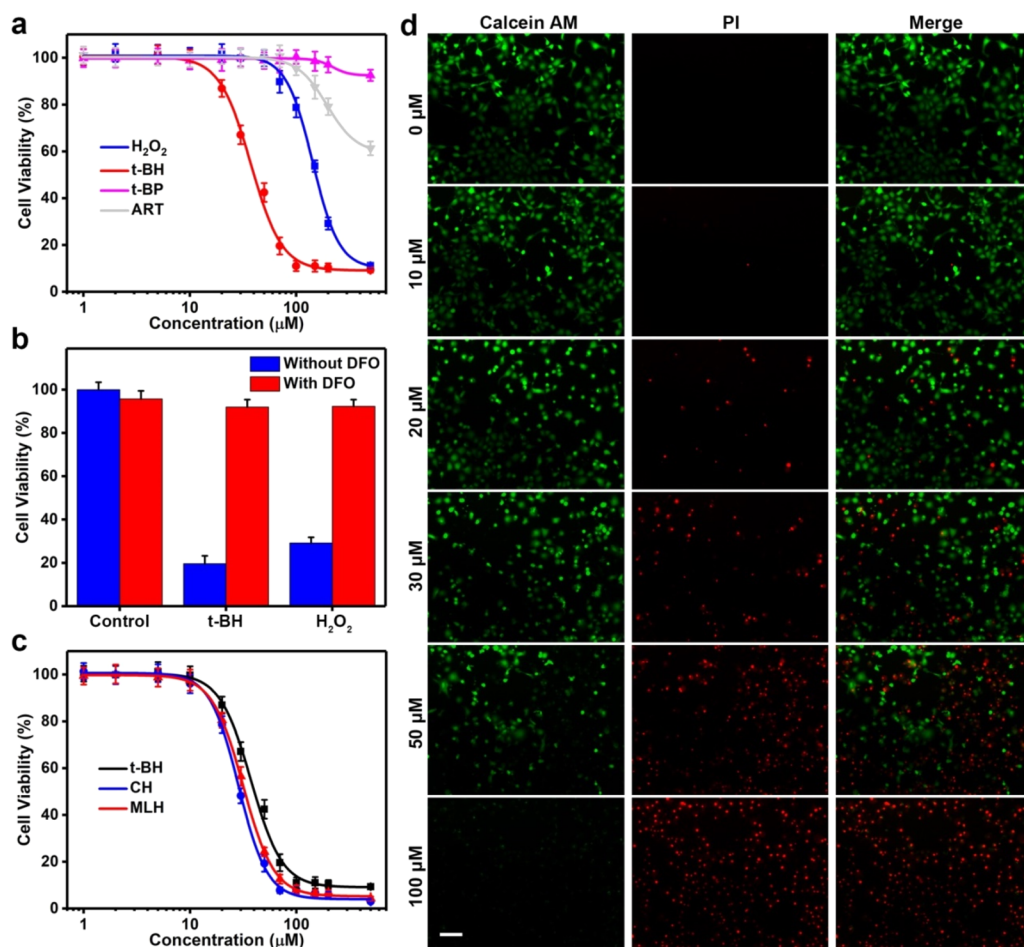


Figure 2. (a) Viability of U87MG cells after exposure to different types of ROOR for 24 h. (b) In vitro CDT cytotoxicity of ROOR with or without iron chelator DFO. [t-BH] = $70 \mu\text{M}$, [H_2O_2] = $200 \mu\text{M}$, [DFO] = $200 \mu\text{M}$. (c) Viability of cancer cells after 24 h of treatment with diverse R'OOH including t-BH, CH, and MLH. IC₅₀ for t-BH, CH, and MLH were 40.2, 29.5, and $32.7 \mu\text{M}$, respectively. (d) Calcein AM/PI costaining of U87MG cells incubated with different concentrations of MLH. Scale bar represents $50 \mu\text{m}$.

that is a typical thiol-containing-biomolecule/corresponding-enzyme pair. In addition to H_2O_2 , *tert*-butyl hydroperoxide (t-BH), *tert*-butyl peroxide (t-BP), and ART were selected as the representatives of R'OOH, R'OOR', and endoperoxides, respectively, to investigate the relative reactivity of diverse ROOR in the above two reaction pathways.

First, the conversion of ROOR into RO• radicals through Fenton chemistry was measured by using 3,3',5,5'-tetramethylbenzidine (TMB) as a probe that is able to produce a blue-green color with an absorption maximum at $\sim 650 \text{ nm}$ upon oxidation by RO• radicals. As shown in Figure 1b and Figure S1, H_2O_2 and t-BH showed effective and comparable ROS generation within 5 min of mixing with Fe^{2+} , in sharp contrast to t-BP or ART. The TMB absorbance was almost not affected by t-BP in the presence of Fe^{2+} , and the endoperoxide ART only induced a slight change in the absorbance of TMB solution even after reaction under the same conditions for 24 h (Figure 1c). In this regard, the chemodynamic efficacy of t-BP and ART against cancer cells would be insufficient owing to their low ROS generation ability. Given the fact that oxidized glutathione (GSSG) is generated during the redox reaction of ROOR with GSH and that GSSG can participate in the oxidation of NADPH to NADP^+ with the catalysis of GSH reductase (GR), a mixture solution containing GSH, GPx, NADPH, and GR was employed to investigate the conversion

of ROOR to ROH by monitoring the decrease in absorbance of NADPH at 340 nm. As can be seen in Figure 1d, the removal rate of ROOR by GSH/GPx decreased in the order of $\text{H}_2\text{O}_2 > \text{t-BH} > \text{t-BP} \approx \text{ART}$, according to the decay curves of NADPH. Importantly, H_2O_2 could be consumed directly by GSH alone, without the addition of GPx (Figure 1e and Figure S2). Rapid consumption of H_2O_2 by GSH or GSH/GPx, together with the fact that it can also be decomposed to H_2O and O_2 by intracellular catalase, would strongly diminish the chemodynamic cytotoxicity of H_2O_2 . Taken together, as compared to other ROOR, R'OOH possesses ideal characteristics, including excellent free radical-producing ability and relatively moderate reactivity with GSH/GPx, to act as a potent chemodynamic agent for realizing LIP-stimulated cancer cell death.

In Vitro Labile Iron-Triggered CDT by ROOR. To assess the chemodynamic activities of ROOR against cancer in vitro, methyl thiazolyl tetrazolium (MTT) assay was carried out to quantify the viability of U87MG cells after 24 h of treatment with various ROOR. As expected, t-BH exhibited a much superior cancer cell killing effect as compared to H_2O_2 , t-BP, and ART (Figure 2a). The rank order of the half-maximal inhibitory concentration (IC₅₀) of different ROOR was t-BH ($40.2 \mu\text{M}$) < H_2O_2 ($153.1 \mu\text{M}$) < ART < t-BP. This finding is consistent with the prediction made by the proposed

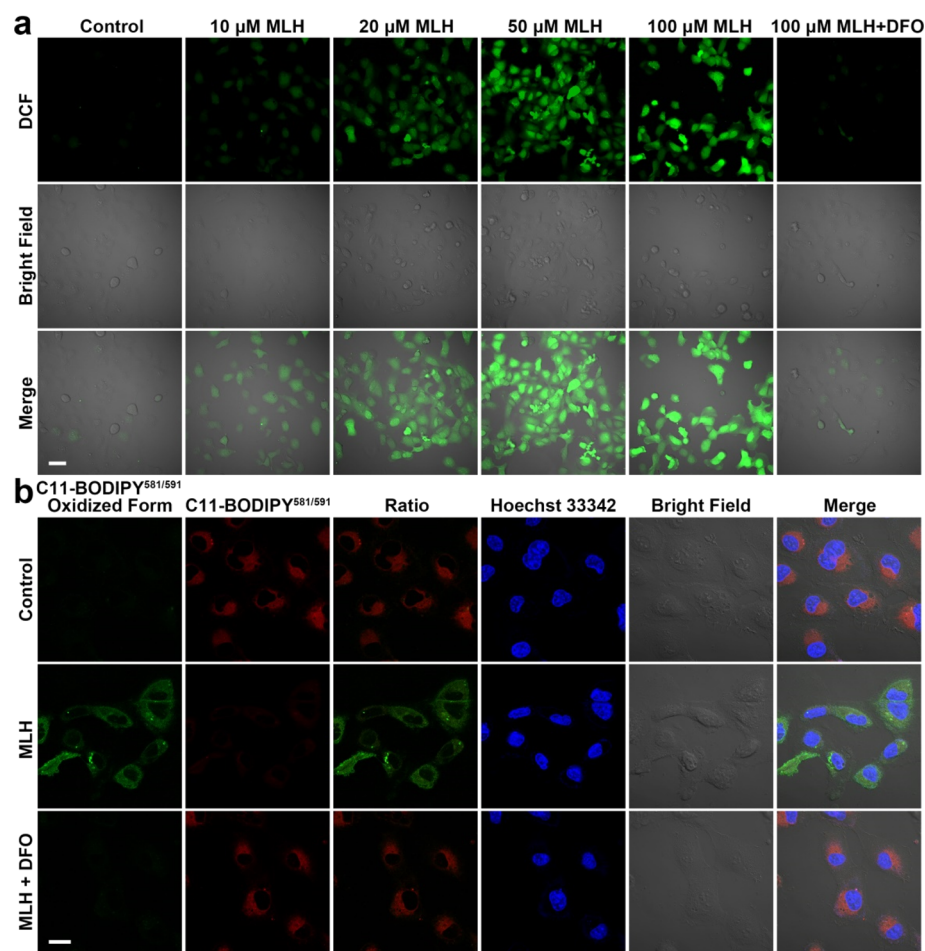


Figure 3. (a) DCF fluorescence of U87MG cells treated with various concentrations of MLH in the presence or absence of 200 μM DFO for 4 h. Scale bar represents 50 μm . (b) Fluorescence images of C11-BODIPY^{581/591}-stained cancer cells after 4 h of exposure to MLH with or without DFO. [MLH] = 100 μM , [DFO] = 200 μM . Scale bar represents 20 μm .

assessment method, which in turn demonstrates the feasibility of the developed method for identifying a ROOR with optimal chemodynamic efficiency. The limited CDT effect of H_2O_2 and ART could be attributed to rapid clearance by GSH/GPx and low free radical-producing ability, respectively. Importantly, no apparent cell death was induced by t-BH in a high concentration when U87MG cells were coincubated with the iron chelator deferoxamine (DFO), as shown in Figure 2b, revealing that the chemodynamic cytotoxicity of R'OOH is activated specifically by intracellular labile iron(II), which could be ascribed to the conversion of less-reactive R'OOH into R'O• radicals by labile iron(II)-triggered Fenton-type reactions. The endogenous LIP-activatable chemodynamic effect, along with the elevated levels of LIP content in cancer cells (Figure S3), allows R'OOH to efficiently and specifically inhibit tumor progression.

To confirm whether various R'OOH with different alkyl groups have similar CDT behavior, we compare the chemodynamic efficacy of diverse R'OOH including t-BH, cumene hydroperoxide (CH), and MLH. The MLH was synthesized through the photosensitized oxidation of methyl linoleate, and the successful preparation of MLH was verified by ^1H and ^{13}C NMR spectroscopy (Figure S4). It can be seen in Figure 2c that all three R'OOH displayed a potent anticancer activity with relatively similar IC₅₀ values, demonstrating that the change of R' group does not significantly alter the CDT

efficiency of R'OOH against cancer cells. The chemodynamic cytotoxicity of all R'OOH was greatly inhibited by iron chelator (Figure S5). The MLH, a lipid hydroperoxide, was selected as the representative R'OOH in the following studies. Then, a live/dead cell costaining assay was performed to intuitively determine the R'OOH-induced cancer cell death. After incubating U87MG cells with different concentrations of MLH for 24 h, calcein AM and propidium iodide (PI) were introduced to label the live and dead cells, respectively. As shown in the fluorescence images (Figure 2d), the proportion of dead cells with red fluorescence increased in a concentration-dependent manner, further confirming the CDT-mediated cancer cell killing ability of MLH.

Therapeutic Mechanism of MLH in Cancer CDT. To gain insights into the mechanism underlying the anticancer action of R'OOH at the cellular level, we examined the LIP-stimulated generation of free radicals from MLH by using 2',7'-dichlorofluorescein diacetate (DCFH-DA) as a fluorescent probe, whose deacetylated form emits green fluorescence in response to ROS.^{38–41} As shown in Figure 3a, a strong green fluorescence was observed in MLH-incubated U87MG cells, but not in untreated control cells, which implied the ability of MLH to generate free radicals inside cells, as a consequence of its participation in the endogenous labile iron(II)-dependent Fenton process. Moreover, the ROS production by MLH was remarkably suppressed through the chelation of labile iron(II)

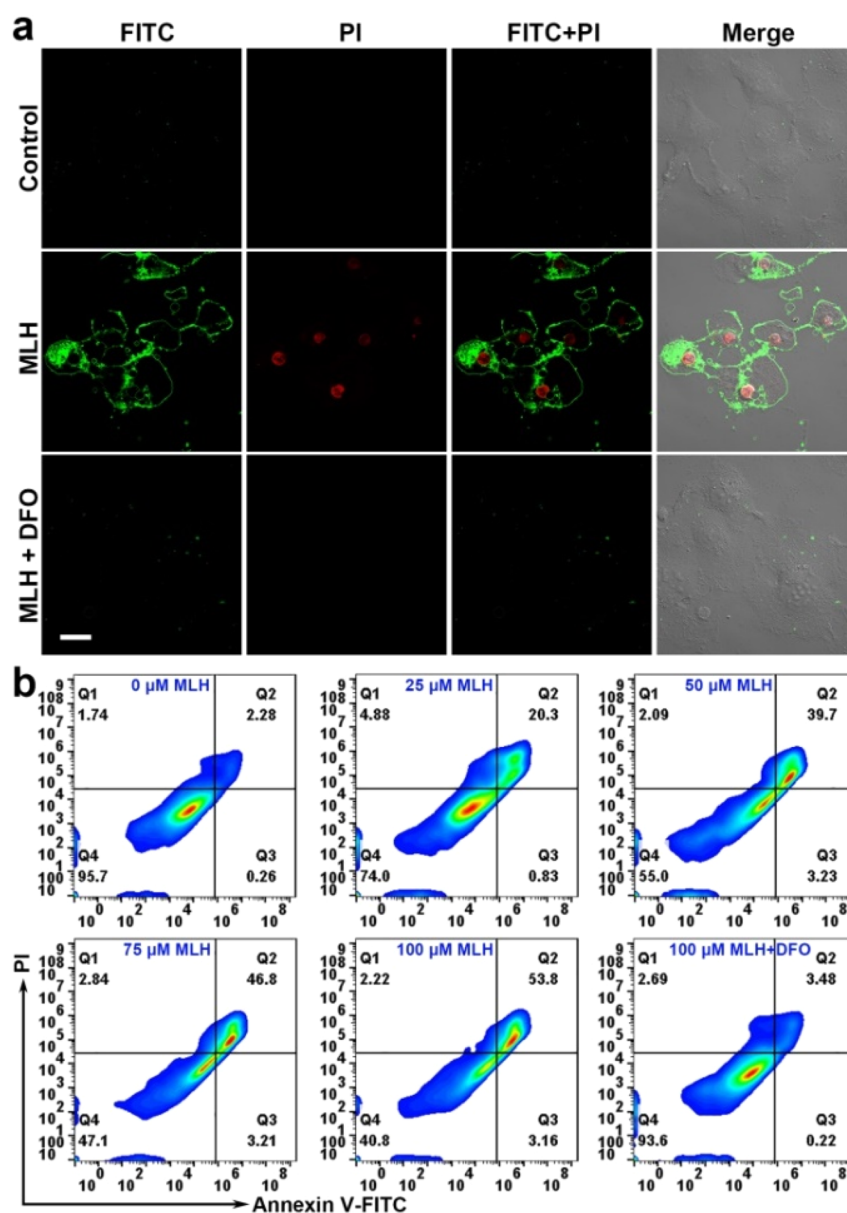


Figure 4. (a) Fluorescence images of annexin V-FITC/PI costained U87MG cells after 24 h of exposure to 100 μM MLH with or without 200 μM DFO. Scale bar represents 20 μm . (b) Flow cytometry analysis of tumor cell apoptosis after 12 h of treatment with different concentrations of MLH.

with DFO, further demonstrating that the transformation of MLH to free radicals is driven by intracellular LIP. Free radicals are known to initiate lipid peroxidation (LPO) and thus result in cell death. Consequently, we selected the dye molecule C11-BODIPY^{581/591} as a ratiometric fluorescent indicator to evaluate the MLH-induced LPO by monitoring its fluorescence shift from red to green. As can be seen in Figure 3b, exposure of U87MG cells to MLH caused a significant decrease in red fluorescence as well as an increase in green fluorescence, clearly suggesting the capacity of MLH to activate LPO through the production of free radicals by Fenton chemistry.

ROS accumulation, along with the ensuing LPO, has been reported to trigger cell apoptosis. The annexin V-FITC/PI kit was utilized to study the effect of MLH on the induction of cancer cell apoptosis. It can be seen in Figure 4a that U87MG cells in CDT group showed strong green and red fluorescence,

whereas negligible fluorescence was detected in untreated control cells and cells treated with MLH plus DFO, suggesting the potential of MLH to promote apoptotic cell death through LIP-mediated mechanism. Flow cytometry was used to further quantitatively determine apoptotic cells. As expected, the MLH stimulated tumor cell apoptosis in a dose-dependent manner (Figure 4b). Importantly, the apoptosis of U87MG cells exposed to MLH were prevented by chelation of intracellular labile iron(II). Furthermore, MLH displayed a lower toxicity toward normal cells, which could be ascribed to the insufficient LIP-triggered ROS production (Figure S6). Taken together, it could be speculated that ROS formation in response to endogenous LIP is one of the most important contributors for the MLH-elicited apoptotic death of cancer cells.

Enhancement of MLH-Based CDT by Increasing Labile Iron(II). Considering that the chemodynamic cytotoxicity of R'OOH is strongly dependent on intracellular labile

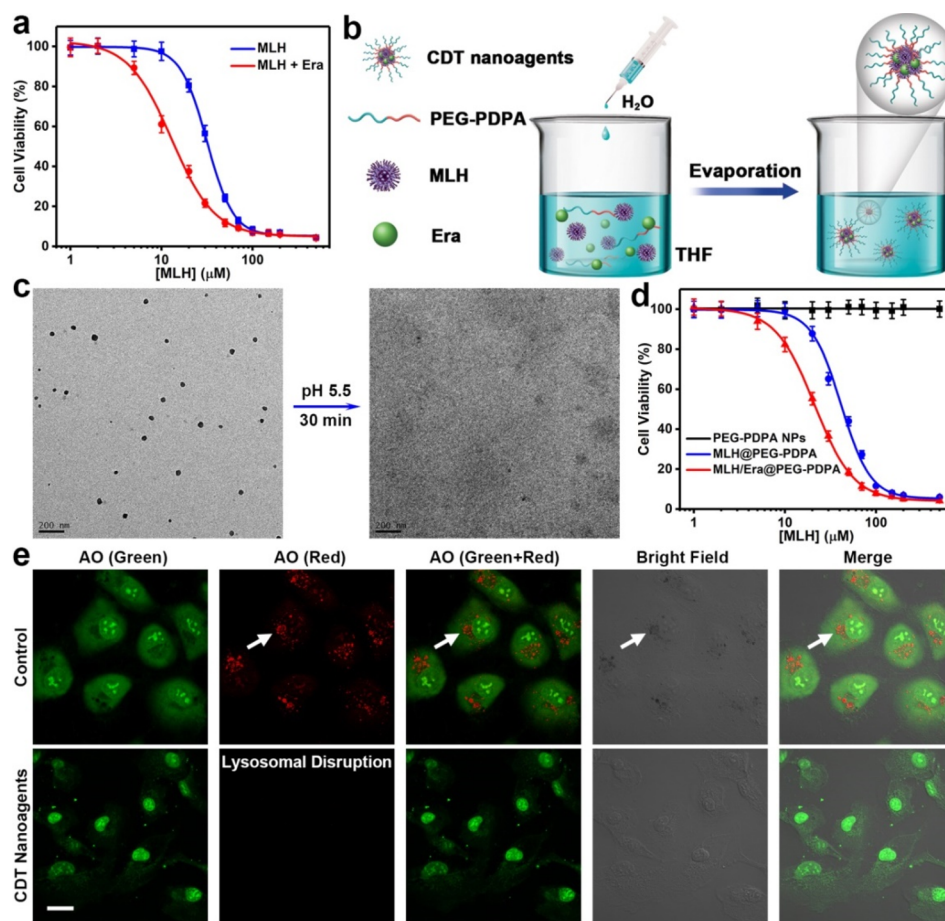


Figure 5. (a) In vitro CDT cytotoxicity of MLH with or without Era as an LIP-increasing agent. [MLH]:[Era] = 10:1. IC₅₀ for MLH alone and MLH plus Era were 32.7 and 14.0 μM , respectively. (b) Schematic illustration of the synthesis of MLH/Era-loaded PEG–PDPA NPs as intensive CDT nanoagents. (c) TEM images of PEG–PDPA NPs after 30 min of dispersion in buffer solutions with pH 7.4 (left) or 5.5 (right). Scale bar represents 200 nm. (d) Viability of U87MG cells after 24 h of treatment with free, MLH-loaded, or MLH/Era-loaded PEG–PDPA NPs. (e) AO staining assay demonstrating lysosomal disruption in U87MG cells exposed to the CDT nanoagents with acid-triggered disassembly property. White arrows point to the AO dye accumulated in intact lysosomes. Scale bar represents 20 μm .

iron(II), we hypothesized that the cotreatment of cancer cells with R'OOH and Era, a small molecule capable of increasing intracellular labile iron(II),⁴² could be an effective strategy for enhanced CDT. To confirm our hypothesis, the viability of U87MG cells exposed to MLH plus Era was determined. Obviously, the combination of MLH with Era showed significant synergistic action on the loss of cell viability with a combination index of 0.82 (Figures 5a, S7, and S8).⁴³ The results verified that the integration of R'OOH with LIP-increasing agent could give rise to reinforced chemodynamic efficacy. Similarly, the synergistic cancer cell destruction was mitigated by DFO coinubation (Figure S9), suggesting that LIP-activated Fenton chemistry is the key mechanism underlying the synergistic cytotoxicity. It is worth noting that these results further highlighted the critical role of labile iron(II) in R'OOH-based anticancer CDT.

Fabrication and Characterization of MLH-Carrying CDT Nanoagents. It is well-known that nanomedicines in the size range of 10–100 nm accumulate preferentially in tumor tissues through the enhanced permeability and retention (EPR) effect. To this end, a CDT nanoagent was constructed by encapsulating MLH and Era into the self-assembled nanostructures of pH-sensitive amphiphilic poly(ethylene glycol)-*block*-poly(diisopropylaminoethyl methacrylate)

(PEG–PDPA) (Figure 5b and Figure S10).⁴⁴ The CDT nanoagents with a loading efficiency of about 97% remained stable in serum (Figure S11). After internalization by tumor cells, the hydrophobic PDPA of PEG–PDPA polymer would become hydrophilic in the acidic endo/lysosomal compartments, leading to the disintegration of the nanovehicles, accompanied by the rapid release of MLH and Era (Figure S12). The pH-responsive disassembly of the as-prepared CDT nanoagents with a diameter of ~ 50 nm, induced by the hydrophobic-to-hydrophilic transition of PDPA upon protonation with acid, was verified by their transmission electron microscopy (TEM) images at different pH values, as shown in Figure 5c. Their small particle size suitable for the EPR effect-driven accumulation in tumors (Figure S13), together with the activatable drug release resulting from their pH-triggered disassembly, allows the CDT nanoagents to achieve specific tumor treatment in vivo.

In Vitro Chemodynamic Cytotoxicity of MLH-Carrying Nanoagents. The CDT toxicity of MLH-carrying nanoagents against tumor cells in vitro was investigated by MTT assay. U87MG cells were incubated with free, MLH-loaded, or MLH/Era-loaded PEG–PDPA NPs for 24 h. As shown in Figure 5d, free PEG–PDPA NPs displayed negligible toxicity to U87MG cells, whereas a significant reduction in cell

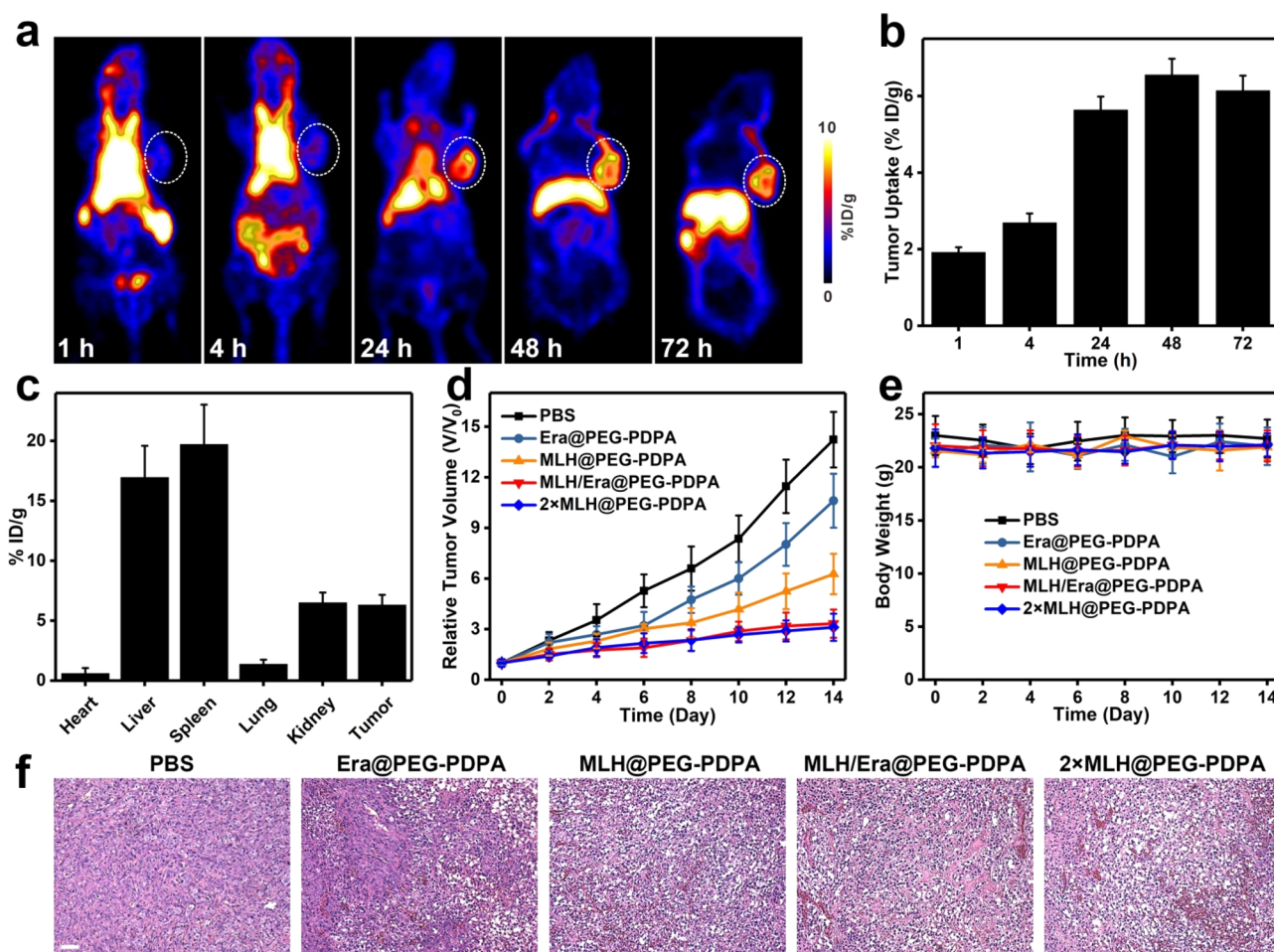


Figure 6. (a) Whole-body coronal PET images of U87MG tumor-bearing mice after intravenous injection of ^{89}Zr -labeled CDT nanoagents. White circles indicate the tumor sites. (b) Tumor uptake of ^{89}Zr -labeled CDT nanoagents measured by PET images. (c) Biodistribution of ^{89}Zr -labeled CDT nanoagents at 72 h postinjection. (d) Tumor growth and (e) body weight curves of mice after different treatments. (f) H&E-stained images of tumor tissues collected from different groups. Scale bar, 100 μm .

viability was observed when cancer cells were treated with MLH-loaded or MLH/Era-loaded PEG-PDPA NPs. The MLH-carrying CDT nanoagents-driven cancer cell injury could be attributed to their disassembly in the acidic environment of endo/lysosomes as well as the accompanied formation of highly deleterious free radicals through the Fenton-type reaction between the released MLH and intracellular labile iron(II).

Previous studies have suggested that ROS can induce the disruption of intracellular organelles. Moreover, the PEG-PDPA NPs were first localized in lysosomes after internalization by cancer cells (Figure S14). Considering the acid-triggered disassembly behavior of PEG-PDPA NPs and the acidic pH of lysosomes, acridine orange (AO) staining assay was performed to determine lysosomal damage by CDT nanoagents. As shown in Figure 5e, a bright red fluorescence resulted from the accumulation of AO in acidic organelles, particularly intact lysosomes, was observed in untreated control cells. The treatment of U87MG cells with MLH/Era-loaded PEG-PDPA NPs led to the disappearance of red fluorescence, indicating the destruction of lysosomes by MLH-carrying CDT nanoagents, which was capable of promoting cancer cell apoptosis (Figure S15).

In Vivo Tumor Treatment with CDT Nanoagents. Given the small particle size of PEG-PDPA NPs, it can be

expected that the prepared CDT nanoagents would accumulate preferentially in tumor tissues by the EPR effect. In order to validate our hypothesis, the in vivo biodistribution of CDT nanoagents in mice bearing U87MG tumors was estimated by positron emission tomography (PET) imaging upon intravenous injection of ^{89}Zr -labeled CDT nanoagents. As can be seen in Figures 6a and S16, the radioactivity in tumor gradually increased after administration. The tumor uptake values were 1.92%, 2.69%, 5.64%, 6.55%, and 6.14% injected dose per gram (ID/g) at 1, 4, 24, 48, and 72 h, respectively (Figure 6b), suggesting effective accumulation of ^{89}Zr -labeled CDT nanoagents in tumor, which could be ascribed to the prolonged blood circulation as well as the EPR effect (Figure S17). The biodistribution data obtained by ex vivo gamma counting further supported the high tumor uptake of CDT nanoagents (Figure 6c).

Encouraged by their potent chemodynamic cytotoxicity against cancer cells and efficient tumor accumulation, we investigated the feasibility of using pH-responsive CDT nanoagents for tumor growth inhibition in vivo. As shown in Figure 6d, the growth of tumors in mice treated with MLH-carrying CDT nanoagents was obviously suppressed compared to the PBS-injected control group, which resulted from the generation of free radicals by intracellular LIP-driven Fenton-type chemistry. Moreover, the integration of MLH with Era

achieved intensive antitumor CDT (Figure S18). In addition, neither obvious body weight loss nor apparent damage in major organs was found in mice after CDT (Figures 6e and S19). The destruction of tumor tissues in CDT groups was further revealed by hematoxylin and eosin (H&E)-stained images (Figure 6f). The above results demonstrated that the MLH-carrying PEG–PDPA NPs are promising CDT agents for endogenous LIP-activated cancer therapy with minimized side effects.

CONCLUSIONS

In summary, we have described a new endogenous LIP-based CDT strategy, and the identification of a ROOR featuring optimal LIP-mediated CDT efficiency as well as its use for fabricating intensive chemodynamic nanoagents as activatable cancer therapeutics. Through simulation of metabolic processes of ROOR inside cells, R'OOH was shown to possess excellent free radical-generating capacity with the help of Fe²⁺ and to be only moderately eliminated by the GSH/GPx system, endowing it with superior chemodynamic efficacy compared to other kinds of ROOR. After uptake by cancer cells with elevated LIP levels, R'OOH could be efficiently converted into the highly deleterious free radicals through the intracellular labile iron(II)-mediated Fenton chemistry, which makes it an activatable CDT agent to elicit tumor cell death. Impressively, the combination of R'OOH and LIP-increasing agent exerted enhanced chemodynamic efficacy against cancer. In addition to preferential accumulation in tumor tissue via the EPR effect, the CDT nanoagents prepared by encapsulating MLH and Era within pH-sensitive polymer particles were able to provide controlled release of cargoes with LIP-stimulated chemodynamic cytotoxicity, enabling them to effectively suppress tumor growth in vivo with minimal side effects. Our work advances the fundamental understanding of the intracellular metabolic pathways of ROOR and provides a paradigm for the exploration of high-performance CDT agents activated by endogenous LIP.

EXPERIMENTAL SECTION

Materials. Hydrogen peroxide (H₂O₂, 30%), *tert*-butyl hydroperoxide (t-BH, 70 wt % in water), *tert*-butyl peroxide (t-BP, 98%), iron(II) chloride (FeCl₂, 98%), glutathione (GSH, 98%), cumene hydroperoxide (CH, 80%), methyl linoleate (98%), methylene blue (MB), thiazolyl blue tetrazolium bromide (MTT, 97.5%), dimethyl sulfoxide (DMSO, 99.9%), propidium iodide (PI, 94%), deferoxamine mesylate salt (DFO, 92.5%), 2',7'-dichlorofluorescein diacetate (DCFH-DA, 97%), and erastin (Era, 98%) were purchased from Sigma-Aldrich. Glutathione peroxidase (GPx) assay kit was obtained from Merck. C11-BODIPY^{581/591}, artemisinin (ART, 98%), 3,3',5,5'-tetramethylbenzidine (TMB, 99%), calcein AM, and dead cell apoptosis kit were purchased from Thermo Fisher Scientific.

Free Radical Generation by ROOR through Fe²⁺-Driven Fenton Chemistry. The solutions containing 100 μM ROOR (t-BH, H₂O₂, t-BP, or ART) and 40 μg mL⁻¹ TMB were mixed with FeCl₂ ([Fe] = 5 μg mL⁻¹) to initiate Fenton-type reactions. The change in absorbance of TMB at 650 nm was monitored to compare the production of free radical by various kinds of ROOR.

Conversion of ROOR to Non-Toxic ROH by GSH/GPx. The clearance of diverse ROOR by GSH/GPx was determined using a GPx assay with a modified protocol. The commercial GPx assay kit contains assay buffer, sample buffer, GPx, and cosubstrate mixture. The cosubstrate mixture is composed of GSH, NADPH, and GR. The GPx-catalyzed reaction of ROOR with GSH can yield oxidized glutathione (GSSG) that further participates in the oxidation of NADPH to NADP⁺ with the assistance of GR. After the addition of

various ROOR (20 μL, 1.9 mM) to a solution containing 110 μL of assay buffer, 10 μL of sample buffer, and 50 μL of cosubstrate mixture, the absorbance decrease of NADPH at 340 nm was measured to assess the removal of ROOR by GSH/GPx.

Synthesis of MLH and MLH-Carrying CDT Nanoagents. The MLH was prepared through the oxidation of methyl linoleate by singlet oxygen generated from MB upon light irradiation. Briefly, 6 g of methyl linoleate and 10 mg of MB were dissolved in 50 mL of dichloromethane. Under a continuous flux of oxygen, the mixture was irradiated with a 671 nm laser (100 mW cm⁻²) for 2 h at 0 °C. Subsequently, MLH was purified by silica gel column chromatography using pure dichloromethane and then dichloromethane/ethyl acetate = 4:1 (v/v).

PEG–PDPA was synthesized according to our previous work.⁴² To fabricate MLH-carrying CDT nanoagents, MLH (40 μL, 100 mM in DMF) and Era (40 μL, 10 mM in DMF) were mixed with a THF solution of PEG–PDPA (3 mL, 8 mg). After dropwise addition of 8 mL of H₂O, the solution containing as-prepared MLH/Era@PEG–PDPA NPs was evaporated to remove organic solvent.

pH-Responsive Disassembly of PEG–PDPA NPs. The PEG–PDPA NPs were dispersed in buffer solutions with different pH values (7.4 or 5.5). After incubation for 30 min, TEM images were taken at the same magnification.

In Vitro Labile Iron(II)-Mediated CDT. First, MTT assay was carried out to quantitatively evaluate the chemodynamic activities of different ROOR against cancer cells. U87MG cells (5 × 10³ cells per well) were seeded in 96-well plates overnight. After treatment with different concentrations of ROOR (H₂O₂, t-BH, t-BP, or ART) for 24 h, U87MG cells were exposed to 1 mg mL⁻¹ MTT for another 4 h. The culture medium was replaced with 150 μL of DMSO, and then the absorbance at 570 nm was recorded. Furthermore, the viability of U87MG cells after exposure to diverse ROOR with or without iron chelator DFO (200 μM) was measured by similar procedures. In addition, the CDT efficacy of different R'OOH (t-BH, CH, or MLH), MLH plus Era ([MLH]:[Era] = 10:1), and various MLH-carrying chemodynamic nanoagents was also assessed by the MTT assay.

Next, live/dead cell costaining assay was applied to intuitively detect CDT-based cancer cell killing. U87MG cells were treated with different concentrations of MLH or MLH plus Era for 24 h. After costaining with 1 μg mL⁻¹ calcein AM and 1 μg mL⁻¹ PI at 37 °C for 30 min, cancer cells were imaged by fluorescence microscopy.

Therapeutic Mechanism of MLH in Cancer CDT. The in vitro generation of highly cytotoxic free radicals from MLH was investigated by using DCFH-DA as a fluorescent indicator. U87MG cancer cells were treated with 100 μM MLH in the absence or presence of 200 μM DFO for 4 h. After incubation of cells with 10 μM DCFH-DA for 30 min, the fluorescence images were collected.

The C11-BODIPY^{581/591} ratiometric fluorescence probe was employed to evaluate MLH-induced lipid peroxidation as a consequence of labile iron(II)-mediated free radical production. After 4 h of exposure to 100 μM MLH with or without 200 μM DFO, U87MG cells were stained with 10 μM C11-BODIPY^{581/591} for 30 min and then with 5 μg mL⁻¹ Hoechst 33342 for 15 min. Finally, the fluorescence shift from red to green was recorded.

MLH-induced apoptotic death of cancer cells was investigated with an apoptosis kit comprising of annexin V-FITC and PI. U87MG cells were treated with 100 μM MLH in the absence or presence of 200 μM DFO for 24 h. Subsequently, the cells were stained with annexin V-FITC/PI following the manufacturer's instructions and then imaged by fluorescence microscopy. Flow cytometry was used to further quantify LIP-mediated apoptotic cells. Similarly, after exposure to various concentrations of MLH for 12 h, U87MG cells were harvested, incubated with annexin V-FITC/PI for 15 min, and then analyzed using a flow cytometer.

Lysosomal Damage Triggered by CDT Nanoagents. U87MG cells were incubated with MLH/Era-loaded CDT nanoagents ([MLH] = 100 μM) for 24 h. After 30 min of staining with 5 μM acridine orange (AO), the cells were imaged with a fluorescence microscope.

In Vivo Chemodynamic Therapy. Positron emission tomography (PET) imaging was utilized to assess the in vivo biodistribution of CDT nanoagents in mice bearing U87MG tumors. The ^{89}Zr labeling was realized by the integration of PEG-PDPA NPs with PEG-DFO-PDPA,⁷ in which DFO is able to chelate ^{89}Zr . Mice bearing U87MG tumors were intravenously injected with 200 μCi ^{89}Zr -labeled CDT nanoagents and then scanned using an Inveon small-animal PET scanner. After the collection of tumors and major organs at 72 h postinjection, the radioactivity was measured by a gamma counter.

To examine in vivo tumor growth inhibition by CDT nanoagents, U87MG tumor-bearing mice were intravenously administrated with PBS, Era@PEG-PDPA NPs ([Era] = 1.5 $\mu\text{mol kg}^{-1}$), MLH@PEG-PDPA NPs ([MLH] = 15 $\mu\text{mol kg}^{-1}$), MLH/Era@PEG-PDPA NPs ([MLH] = 15 $\mu\text{mol kg}^{-1}$, [Era] = 1.5 $\mu\text{mol kg}^{-1}$), or 2 \times MLH@PEG-PDPA NPs ([MLH] = 30 $\mu\text{mol kg}^{-1}$) every other day for four doses. Both the body weight and tumor volume were measured during the observation period.

■ ASSOCIATED CONTENT

SI Supporting Information

The Supporting Information is available free of charge at <https://pubs.acs.org/doi/10.1021/jacs.0c05604>.

Additional experimental results as presented in Figures S1–S19 (PDF)

■ AUTHOR INFORMATION

Corresponding Authors

Zhi-Yi Chen – Department of Ultrasound Medicine, Laboratory of Ultrasound Molecular Imaging, The Third Affiliated Hospital of Guangzhou Medical University, Guangzhou 510150, China; orcid.org/0000-0002-5498-5349; Email: wincen@vip.126.com

Xiaoyuan Chen – Laboratory of Molecular Imaging and Nanomedicine (LOMIN), National Institute of Biomedical Imaging and Bioengineering (NIBIB), National Institutes of Health (NIH), Bethesda, Maryland 20892, United States; orcid.org/0000-0002-9622-0870; Email: chen9647@gmail.com

Authors

Lisen Lin – Department of Ultrasound Medicine, Laboratory of Ultrasound Molecular Imaging, The Third Affiliated Hospital of Guangzhou Medical University, Guangzhou 510150, China; MOE Key Laboratory for Analytical Science of Food Safety and Biology & Institute of Environmental Analysis and Detection, College of Chemistry, Fuzhou University, Fuzhou 350108, China; Laboratory of Molecular Imaging and Nanomedicine (LOMIN), National Institute of Biomedical Imaging and Bioengineering (NIBIB), National Institutes of Health (NIH), Bethesda, Maryland 20892, United States

Sheng Wang – School of Life Sciences, Tianjin University and Tianjin Engineering Center of Micro-Nano Biomaterials and Detection-Treatment Technology, Tianjin 300072, China; orcid.org/0000-0002-4797-5310

Hongzhang Deng – Laboratory of Molecular Imaging and Nanomedicine (LOMIN), National Institute of Biomedical Imaging and Bioengineering (NIBIB), National Institutes of Health (NIH), Bethesda, Maryland 20892, United States; orcid.org/0000-0003-3637-8905

Weijing Yang – Laboratory of Molecular Imaging and Nanomedicine (LOMIN), National Institute of Biomedical Imaging and Bioengineering (NIBIB), National Institutes of Health (NIH), Bethesda, Maryland 20892, United States

Lang Rao – Laboratory of Molecular Imaging and Nanomedicine (LOMIN), National Institute of Biomedical Imaging and Bioengineering (NIBIB), National Institutes of Health (NIH), Bethesda, Maryland 20892, United States

Rui Tian – Laboratory of Molecular Imaging and Nanomedicine (LOMIN), National Institute of Biomedical Imaging and Bioengineering (NIBIB), National Institutes of Health (NIH), Bethesda, Maryland 20892, United States

Yuan Liu – Laboratory of Molecular Imaging and Nanomedicine (LOMIN), National Institute of Biomedical Imaging and Bioengineering (NIBIB), National Institutes of Health (NIH), Bethesda, Maryland 20892, United States

Guocan Yu – Laboratory of Molecular Imaging and Nanomedicine (LOMIN), National Institute of Biomedical Imaging and Bioengineering (NIBIB), National Institutes of Health (NIH), Bethesda, Maryland 20892, United States

Zijian Zhou – Laboratory of Molecular Imaging and Nanomedicine (LOMIN), National Institute of Biomedical Imaging and Bioengineering (NIBIB), National Institutes of Health (NIH), Bethesda, Maryland 20892, United States

Jibin Song – MOE Key Laboratory for Analytical Science of Food Safety and Biology & Institute of Environmental Analysis and Detection, College of Chemistry, Fuzhou University, Fuzhou 350108, China; orcid.org/0000-0003-4771-5006

Huang-Hao Yang – MOE Key Laboratory for Analytical Science of Food Safety and Biology & Institute of Environmental Analysis and Detection, College of Chemistry, Fuzhou University, Fuzhou 350108, China; orcid.org/0000-0001-5894-0909

Complete contact information is available at: <https://pubs.acs.org/10.1021/jacs.0c05604>

Author Contributions

[†]L.L. and S.W. contributed equally to this work.

Notes

The authors declare no competing financial interest.

■ ACKNOWLEDGMENTS

This work was supported by National Natural Science Foundation of China (Nos. 81971621 and 81671707), Natural Science Foundation of Guangdong Province (No. 2019A1515012212), Research Fund for Lin He's Academician Workstation of New Medicine and Clinical Translation, and the Intramural Research Program (IRP) of the NIBIB, NIH.

■ REFERENCES

- (1) Zhang, C.; Bu, W.; Ni, D.; Zhang, S.; Li, Q.; Yao, Z.; Zhang, J.; Yao, H.; Wang, Z.; Shi, J. Synthesis of Iron Nanometallic Glasses and Their Application in Cancer Therapy by a Localized Fenton Reaction. *Angew. Chem., Int. Ed.* **2016**, *55*, 2101–2106.
- (2) Ma, B.; Wang, S.; Liu, F.; Zhang, S.; Duan, J.; Li, Z.; Kong, Y.; Sang, Y.; Liu, H.; Bu, W.; Li, L. Self-Assembled Copper-Amino Acid Nanoparticles for in Situ Glutathione “AND” H_2O_2 Sequentially Triggered Chemodynamic Therapy. *J. Am. Chem. Soc.* **2019**, *141*, 849–857.
- (3) Liu, G.; Zhu, J.; Guo, H.; Sun, A.; Chen, P.; Xi, L.; Huang, W.; Song, X.; Dong, X. Mo_2C -Derived Polyoxometalate for NIR-II Photoacoustic Imaging-Guided Chemodynamic/Photothermal Synergistic Therapy. *Angew. Chem., Int. Ed.* **2019**, *58*, 18641–18646.
- (4) Lin, L.-S.; Huang, T.; Song, J.; Ou, X.-Y.; Wang, Z.; Deng, H.; Tian, R.; Liu, Y.; Wang, J.-F.; Liu, Y.; Yu, G.; Zhou, Z.; Wang, S.; Niu, G.; Yang, H.-H.; Chen, X. Synthesis of Copper Peroxide Nanodots for H_2O_2 Self-Supplying Chemodynamic Therapy. *J. Am. Chem. Soc.* **2019**, *141*, 9937–9945.

- (5) Zhang, L.; Wan, S.-S.; Li, C.-X.; Xu, L.; Cheng, H.; Zhang, X.-Z. An Adenosine Triphosphate-Responsive Autocatalytic Fenton Nanoparticle for Tumor Ablation with Self-Supplied H₂O₂ and Acceleration of Fe(III)/Fe(II) Conversion. *Nano Lett.* **2018**, *18*, 7609–7618.
- (6) Sang, Y.; Cao, F.; Li, W.; Zhang, L.; You, Y.; Deng, Q.; Dong, K.; Ren, J.; Qu, X. Bioinspired Construction of a Nanozyme-Based H₂O₂ Homeostasis Disruptor for Intensive Chemodynamic Therapy. *J. Am. Chem. Soc.* **2020**, *142*, 5177–5183.
- (7) Wang, S.; Yu, G.; Wang, Z.; Jacobson, O.; Lin, L.-S.; Yang, W.; Deng, H.; He, Z.; Liu, Y.; Chen, Z.-Y.; Chen, X. Enhanced Antitumor Efficacy by a Cascade of Reactive Oxygen Species Generation and Drug Release. *Angew. Chem., Int. Ed.* **2019**, *58*, 14758–14763.
- (8) Ranji-Burachaloo, H.; Gurr, P. A.; Dunstan, D. E.; Qiao, G. G. Cancer Treatment through Nanoparticle-Facilitated Fenton Reaction. *ACS Nano* **2018**, *12*, 11819–11837.
- (9) Hu, X.; Li, F.; Xia, F.; Guo, X.; Wang, N.; Liang, L.; Yang, B.; Fan, K.; Yan, X.; Ling, D. Biodegradation-Mediated Enzymatic Activity-Tunable Molybdenum Oxide Nanourchins for Tumor-Specific Cascade Catalytic Therapy. *J. Am. Chem. Soc.* **2020**, *142*, 1636–1644.
- (10) Kim, J.; Cho, H. R.; Jeon, H.; Kim, D.; Song, C.; Lee, N.; Choi, S. H.; Hyeon, T. Continuous O₂-Evolving MnFe₂O₄ Nanoparticle-Anchored Mesoporous Silica Nanoparticles for Efficient Photodynamic Therapy in Hypoxic Cancer. *J. Am. Chem. Soc.* **2017**, *139*, 10992–10995.
- (11) Luby, B. M.; Walsh, C. D.; Zheng, G. Advanced Photosensitizer Activation Strategies for Smarter Photodynamic Therapy Beacons. *Angew. Chem., Int. Ed.* **2019**, *58*, 2558–2569.
- (12) Huang, L.; Li, Z.; Zhao, Y.; Zhang, Y.; Wu, S.; Zhao, J.; Han, G. Ultralow-Power Near Infrared Lamp Light Operable Targeted Organic Nanoparticle Photodynamic Therapy. *J. Am. Chem. Soc.* **2016**, *138*, 14586–14591.
- (13) Lin, L.-S.; Cong, Z.-X.; Li, J.; Ke, K.-M.; Guo, S.-S.; Yang, H.-H.; Chen, G.-N. Graphitic-phase C₃N₄ Nanosheets as Efficient Photosensitizers and pH-Responsive Drug Nanocarriers for Cancer Imaging and Therapy. *J. Mater. Chem. B* **2014**, *2*, 1031–1037.
- (14) Lan, G.; Ni, K.; Veroneau, S. S.; Feng, X.; Nash, G. T.; Luo, T.; Xu, Z.; Lin, W. Titanium-Based Nanoscale Metal-Organic Framework for Type I Photodynamic Therapy. *J. Am. Chem. Soc.* **2019**, *141*, 4204–4208.
- (15) Li, X.; Lee, D.; Huang, J.-D.; Yoon, J. Phthalocyanine-Assembled Nanodots as Photosensitizers for Highly Efficient Type I Photoreactions in Photodynamic Therapy. *Angew. Chem., Int. Ed.* **2018**, *57*, 9885–9890.
- (16) Lovell, J. F.; Liu, T. W. B.; Chen, J.; Zheng, G. Activatable Photosensitizers for Imaging and Therapy. *Chem. Rev.* **2010**, *110*, 2839–2857.
- (17) Lin, L.-S.; Song, J.; Yang, H.-H.; Chen, X. Yolk-Shell Nanostructures: Design, Synthesis, and Biomedical Applications. *Adv. Mater.* **2018**, *30*, 1704639.
- (18) Bai, J.; Jia, X.; Zhen, W.; Cheng, W.; Jiang, X. A Facile Ion-Doping Strategy to Regulate Tumor Microenvironments for Enhanced Multimodal Tumor Theranostics. *J. Am. Chem. Soc.* **2018**, *140*, 106–109.
- (19) Liu, Y.; Ji, X.; Tong, W. W. L.; Askhatova, D.; Yang, T.; Cheng, H.; Wang, Y.; Shi, J. Engineering Multifunctional RNAi Nanomedicine To Concurrently Target Cancer Hallmarks for Combinatorial Therapy. *Angew. Chem., Int. Ed.* **2018**, *57*, 1510–1513.
- (20) Ma, P.; Xiao, H.; Yu, C.; Liu, J.; Cheng, Z.; Song, H.; Zhang, X.; Li, C.; Wang, J.; Gu, Z.; Lin, J. Enhanced Cisplatin Chemotherapy by Iron Oxide Nanocarrier-Mediated Generation of Highly Toxic Reactive Oxygen Species. *Nano Lett.* **2017**, *17*, 928–937.
- (21) Dong, Z.; Feng, L.; Chao, Y.; Hao, Y.; Chen, M.; Gong, F.; Han, X.; Zhang, R.; Cheng, L.; Liu, Z. Amplification of Tumor Oxidative Stresses with Liposomal Fenton Catalyst and Glutathione Inhibitor for Enhanced Cancer Chemotherapy and Radiotherapy. *Nano Lett.* **2019**, *19*, 805–815.
- (22) Lin, L.-S.; Song, J.; Song, L.; Ke, K.; Liu, Y.; Zhou, Z.; Shen, Z.; Li, J.; Yang, Z.; Tang, W.; Niu, G.; Yang, H.-H.; Chen, X. Simultaneous Fenton-like Ion Delivery and Glutathione Depletion by MnO₂-Based Nanoagent to Enhance Chemodynamic Therapy. *Angew. Chem., Int. Ed.* **2018**, *57*, 4902–4906.
- (23) Liu, Y.; Zhen, W.; Wang, Y.; Liu, J.; Jin, L.; Zhang, T.; Zhang, S.; Zhao, Y.; Song, S.; Li, C.; Zhu, J.; Yang, Y.; Zhang, H. One-Dimensional Fe₂P Acts as a Fenton Agent in Response to NIR II Light and Ultrasound for Deep Tumor Synergetic Theranostics. *Angew. Chem., Int. Ed.* **2019**, *58*, 2407–2412.
- (24) Xuan, W.; Xia, Y.; Li, T.; Wang, L.; Liu, Y.; Tan, W. Molecular Self-Assembly of Bioorthogonal Aptamer-Prodrug Conjugate Micelles for Hydrogen Peroxide and pH-Independent Cancer Chemodynamic Therapy. *J. Am. Chem. Soc.* **2020**, *142*, 937–944.
- (25) Cao, Z.; Zhang, L.; Liang, K.; Cheong, S.; Boyer, C.; Gooding, J. J.; Chen, Y.; Gu, Z. Biodegradable 2D Fe-Al Hydroxide for Nanocatalytic Tumor-Dynamic Therapy with Tumor Specificity. *Adv. Sci.* **2018**, *5*, 1801155.
- (26) Li, S.; Shang, L.; Xu, B.; Wang, S.; Gu, K.; Wu, Q.; Sun, Y.; Zhang, Q.; Yang, H.; Zhang, F.; Gu, L.; Zhang, T.; Liu, H. A Nanozyme with Photo-Enhanced Dual Enzyme-Like Activities for Deep Pancreatic Cancer Therapy. *Angew. Chem., Int. Ed.* **2019**, *58*, 12624–12631.
- (27) Yang, Y.; Tang, J.; Abbaraju, P. L.; Jambhrunkar, M.; Song, H.; Zhang, M.; Lei, C.; Fu, J.; Gu, Z.; Liu, Y.; Yu, C. Hybrid Nanoreactors: Enabling an Off-the-Shelf Strategy for Concurrently Enhanced Chemo-immunotherapy. *Angew. Chem., Int. Ed.* **2018**, *57*, 11764–11769.
- (28) Liu, C.; Wang, D.; Zhang, S.; Cheng, Y.; Yang, F.; Xing, Y.; Xu, T.; Dong, H.; Zhang, X. Biodegradable Biomimic Copper/Manganese Silicate Nanospheres for Chemodynamic/Photodynamic Synergistic Therapy with Simultaneous Glutathione Depletion and Hypoxia Relief. *ACS Nano* **2019**, *13*, 4267–4277.
- (29) Torti, S. V.; Torti, F. M. Iron and Cancer: More Ore to be Mined. *Nat. Rev. Cancer* **2013**, *13*, 342–355.
- (30) Kakhlon, O.; Cabantchik, Z. The Labile Iron Pool: Characterization, Measurement, and Participation in Cellular Processes. *Free Radical Biol. Med.* **2002**, *33*, 1037–1046.
- (31) Torti, S. V.; Torti, F. M. Ironing Out Cancer. *Cancer Res.* **2011**, *71*, 1511–1514.
- (32) Pinnix, Z. K.; Miller, L. D.; Wang, W.; D'Agostino, R.; Kute, T.; Willingham, M. C.; Hatcher, H.; Tesfay, L.; Sui, G.; Di, X.; Torti, S. V.; Torti, F. M. Ferroportin and Iron Regulation in Breast Cancer Progression and Prognosis. *Sci. Transl. Med.* **2010**, *2*, 43ra56.
- (33) Schoenfeld, J. D.; Sibenaller, Z. A.; Mapuskar, K. A.; Wagner, B. A.; Cramer-Morales, K. L.; Furqan, M.; Sandhu, S.; Carlisle, T. L.; Smith, M. C.; Abu Hejleh, T.; Berg, D. J.; Zhang, J.; Keech, J.; Parekh, K. R.; Bhatia, S.; Monga, V.; Bodeker, K. L.; Ahmann, L.; Vollstedt, S.; Brown, H.; Shanahan Kauffman, E. P.; Schall, M. E.; Hohl, R. J.; Clamon, G. H.; Greenlee, J. D.; Howard, M. A.; Schultz, M. K.; Smith, B. J.; Riley, D. P.; Domann, F. E.; Cullen, J. J.; Buettner, G. R.; Buatti, J. M.; Spitz, D. R.; Allen, B. G. O₂⁻ and H₂O₂-Mediated Disruption of Fe Metabolism Causes the Differential Susceptibility of NSCLC and GBM Cancer Cells to Pharmacological Ascorbate. *Cancer Cell* **2017**, *31*, 487–500.
- (34) Sciegienka, S. J.; Solst, S. R.; Falls, K. C.; Schoenfeld, J. D.; Klinger, A. R.; Ross, N. L.; Rodman, S. N.; Spitz, D. R.; Fath, M. A. D-penicillamine Combined with Inhibitors of Hydroperoxide Metabolism Enhances Lung and Breast Cancer Cell Responses to Radiation and Carboplatin via H₂O₂-Mediated Oxidative Stress. *Free Radical Biol. Med.* **2017**, *108*, 354–361.
- (35) Walling, C. Fenton's Reagent Revisited. *Acc. Chem. Res.* **1975**, *8*, 125–131.
- (36) Klayman, D. L. Qinghaosu (Artemisinin): An Antimalarial Drug from China. *Science* **1985**, *228*, 1049–1055.
- (37) Meshnick, S. R.; Yang, Y. Z.; Lima, V.; Kuypers, F.; Kamchonwongpaisan, S.; Yuthavong, Y. Iron-Dependent Free Radical Generation from the Antimalarial Agent Artemisinin (Qinghaosu). *Antimicrob. Agents Chemother.* **1993**, *37*, 1108–1114.

(38) Fan, J.-X.; Peng, M.-Y.; Wang, H.; Zheng, H.-R.; Liu, Z.-L.; Li, C.-X.; Wang, X.-N.; Liu, X.-H.; Cheng, S.-X.; Zhang, X.-Z. Engineered Bacterial Bioreactor for Tumor Therapy via Fenton-Like Reaction with Localized H₂O₂ Generation. *Adv. Mater.* **2019**, *31*, 1808278.

(39) Lin, L.-S.; Wang, J.-F.; Song, J.; Liu, Y.; Zhu, G.; Dai, Y.; Shen, Z.; Tian, R.; Song, J.; Wang, Z.; Tang, W.; Yu, G.; Zhou, Z.; Yang, Z.; Huang, T.; Niu, G.; Yang, H.-H.; Chen, Z.-Y.; Chen, X. Cooperation of Endogenous and Exogenous Reactive Oxygen Species Induced by Zinc Peroxide Nanoparticles to Enhance Oxidative Stress-Based Cancer Therapy. *Theranostics* **2019**, *9*, 7200–7209.

(40) Wen, M.; Ouyang, J.; Wei, C.; Li, H.; Chen, W.; Liu, Y.-N. Artificial Enzyme Catalyzed Cascade Reactions: Antitumor Immunotherapy Reinforced by NIR-II Light. *Angew. Chem., Int. Ed.* **2019**, *58*, 17425–17432.

(41) Wu, W.; Yu, L.; Jiang, Q.; Huo, M.; Lin, H.; Wang, L.; Chen, Y.; Shi, J. Enhanced Tumor-Specific Disulfiram Chemotherapy by In Situ Cu²⁺ Chelation-Initiated Nontoxicity-to-Toxicity Transition. *J. Am. Chem. Soc.* **2019**, *141*, 11531–11539.

(42) Alvarez, S. W.; Sviderskiy, V. O.; Terzi, E. M.; Papagiannakopoulos, T.; Moreira, A. L.; Adams, S.; Sabatini, D. M.; Birsoy, K.; Possemato, R. NFS1 Undergoes Positive Selection in Lung Tumours and Protects Cells from Ferroptosis. *Nature* **2017**, *551*, 639–643.

(43) Zhao, L.; Wientjes, M. G.; Au, J. L.-S. Evaluation of Combination Chemotherapy: Integration of Nonlinear Regression, Curve Shift, Isobologram, and Combination Index Analyses. *Clin. Cancer Res.* **2004**, *10*, 7994–8004.

(44) Wang, S.; Wang, Z.; Yu, G.; Zhou, Z.; Jacobson, O.; Liu, Y.; Ma, Y.; Zhang, F.; Chen, Z.-Y.; Chen, X. Tumor-Specific Drug Release and Reactive Oxygen Species Generation for Cancer Chemo/Chemodynamic Combination Therapy. *Adv. Sci.* **2019**, *6*, 1801986.